Available online at www.sciencedirect.com
SCIENCE DIRECT®
International Journal of Solids and Structures 42 (2005) 1797–1817
INTERNATIONAL JOURNAL OF SOLIDS and STRUCTURES
www.elsevier.com/locate/ijsolstr

A micromechanical method to predict the fracture toughness of cellular materials

Sukjoo Choi, Bhavani V. Sankar *

Department of Mechanical and Aerospace Engineering, 231 MAE-A Building, P.O. Box 116250, University of Florida, Gainesville, FL 32611-6250, USA

Received 24 November 2003; received in revised form 20 August 2004
Available online 28 October 2004

Abstract

The Mode I, Mode II and mixed mode fracture toughness of a cellular medium is predicted by simulating the crack propagation using a finite element model. Displacement boundary conditions are applied such that they correspond to a given value of stress intensity factor in a homogeneous solid that has the same elastic constants as the cellular medium. The crack propagation is simulated by breaking the crack tip strut when the maximum stress in that strut exceeds the strength of the strut material. Based on the finite element results a semi-empirical formula is also derived to predict the Mode I and Mode II fracture toughness of cellular solids as a function of relative density. The results show that the displacements and stresses in the foam near the crack tip are very similar to that in an equivalent homogeneous material, and continuum fracture mechanics concepts can be applied to predict the fracture of a cellular medium. The forces acting in the crack tip strut can be considered as the resultant of stresses over an effective length in the corresponding continuum model. A relation for this effective length has been derived in terms of the relative density of the cellular medium.

Keywords: Carbon foam; Cellular solids; Finite element method; Fracture toughness; Micromechanics; Mixed mode fracture; Orthotropic materials

1. Introduction

Cellular materials are made up of a network of beam or plate structures leaving an open space or cell in between. Cellular materials, e.g., carbon and polymeric foams, offer several advantages such as thermal

* Corresponding author. Tel.: +1 352 392 6749; fax: +1 352 392 7303.
E-mail addresses: choi0027@ufl.edu (S. Choi), sankar@ufl.edu (B.V. Sankar).

0020-7683/$ - see front matter © 2004 Elsevier Ltd. All rights reserved.
doi:10.1016/j.ijsolstr.2004.08.021

resistance, durability, low density, impact damage tolerance and cost effectiveness. They have great potential as core materials in sandwich construction, which has application in heat exchangers and thermal protection systems in military and commercial aerospace structures.

An excellent treatise on the structure and properties of cellular solids has been written by Gibson and Ashby (1988). While analytical methods for predicting thermal and thermo-mechanical properties of cellular media are well documented, research on fracture behavior of various foams is still in its infancy. Gibson and Ashby (1988) have presented approximate formulas for Mode I fracture toughness of cellular solids in terms of their relative density and tensile strength of the strut or ligament material. These are limited to cracks parallel to the principal material direction. Moreover, fracture behavior under mixed mode was not studied. In order to estimate the fracture toughness, the stresses in the crack-tip strut (first unbroken cell edge) is calculated in terms of the stress intensity factor. Then the maximum stress in the strut due to the bending moment is equated to the tensile strength of the strut material. The stress intensity factor that would produce such a bending moment is taken as the fracture toughness of the foam.

The SEM micrograph of carbon foam is shown in Fig. 1. The open-cell foam has irregularly sized and spaced cells. For high-density carbon foam (300–800 kg/m^3), the length of cell edges is found to be in the range of 1–2 mm. For low-density carbon foam (160–300 kg/m^3), the cell length is in the range of 200–600 μm. Unit cells of foams have been modeled as tetrakaidecahedra (a polyhedron containing 14 faces, 36 edges and 24 vertices). Li et al. (2003) modeled the open-cell carbon foam as a space frame and calculated the homogeneous elastic constants analytically. They performed a parametric study to understand how the variation in ligament properties affected the elastic constants of the foam. Sihn and Roy (2003) used three-dimensional finite elements to model the unit-cell of the carbon foam and studied the effects of anisotropy in the ligament material on the overall properties of the foam. In the present study the unit cell of the cellular solid is assumed to be a rectangular prism (actually a cube with side c), and the edges or the struts are assumed to have a square cross-section ($h \times h$) as shown in Fig. 2. It should be mentioned that the purpose of the present study is to understand the effects of cell length and strut size on the fracture toughness of a model-foam. The fracture toughness of the carbon foam shown in Fig. 1 was studied experimentally and analytically in Choi and Sankar (2003).

On the macroscale, the cellular solid is considered as a homogeneous orthotropic material. A crack parallel to one of the principal material directions is assumed to exist in the solid and a small region surrounding the crack tip is modeled using Euler–Bernoulli beam finite elements. The commercial finite element software ABAQUS® was used for this purpose. The strut material is assumed to be isotropic, linearly elastic and brittle, and its elastic constants and tensile strength are assumed known. The crack is modeled by breaking several struts along the line of the intended crack. The properties of the strut material in this study are close to that of carbon foam investigated in a previous experimental study (Choi and Sankar, 2003), and they are given in Table 1.

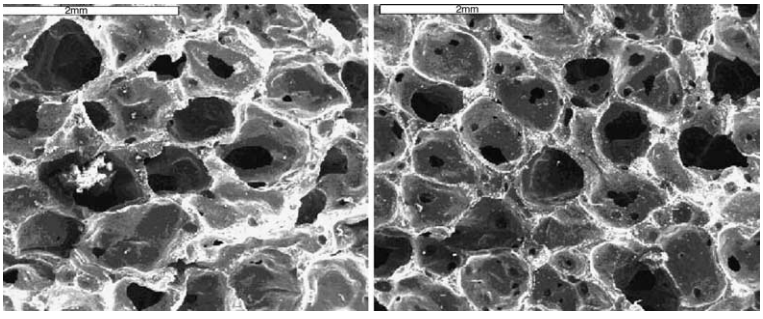

Fig. 1. SEM images of low (left) and high (right) density carbon foam.

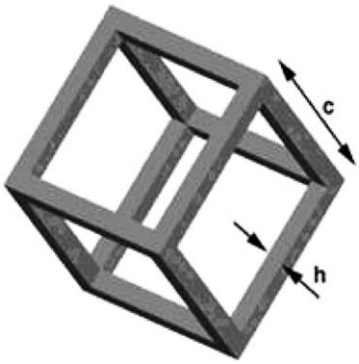

Fig. 2. Open rectangular cell model. The uni-cell is assumed to be a cube of dimension c and the struts (cell edges) are assumed to have a square cross-section $h \times h$.

Table 1
Material properties of the strut material

Density	1750 kg/m^3
Young's modulus	207 GPa
Poisson's ratio	0.17
Ultimate tensile strength	3600 MPa

2. Elastic constants of the foam

As will be seen later, the fracture models require knowledge of the orthotropic properties of the foam. In this section, formulas based on mechanics of materials type calculations for Young's modulus and shear modulus are presented and the results are verified by finite element models. The cellular medium is assumed to consist of struts of square cross-section in a rectangular array in the 1–2 plane. In the following, a superscript * denotes the macroscopic properties of the foam, whereas a subscript s denotes the properties of the strut material.

2.1. Analytical model for elastic constants

The Young's modulus in the principal material direction can be easily derived by subjecting the foam to a state of uniaxial stress σ^* as shown in Fig. 3. The total tensile force acting on a strut is given by $F = c^2\sigma^*$, where c is the length of the unit cell. The microstresses (actual stress) in the strut can be derived as

$$\sigma_s = \frac{F}{h^2} = \frac{c^2\sigma^*}{h^2} \tag{1}$$

where h is the cross-sectional dimension of the square strut (see Fig. 3). It should be noted that both the macrostrain ε^* and microstrain ε must be equal. The microscale strain is given by $\varepsilon_s = \sigma_s/E_s$ and the macroscale strain is $\varepsilon^* = \frac{\sigma^*}{E^*}$. Equating the macro- and microstrains, and using Eq. (1) one can derive a simple formula for the foam Young's modulus E^* as

$$E^* = \left(\frac{h}{c}\right)^2 E_s \tag{2}$$

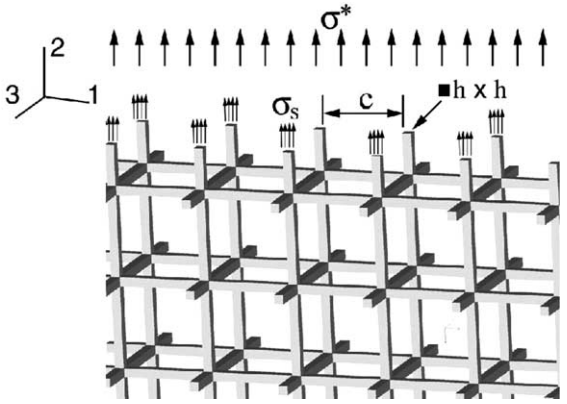

Fig. 3. The cellular medium subjected to a uniform macrostress σ^*. The struts are assumed to have a square cross-section $h \times h$ with a spacing of c in between them.

To calculate the shear modulus G_{12} the unit-cell is subjected to a state of uniform shear as shown in Fig. 4. The deformed shape of the struts is shown in thin lines. Due to anti-symmetry, the curvature of the deformed beam at the center of the strut must be equal to zero and hence the bending moment at the center of the strut must be equal to zero. This fact can be used to find a relation between the force F and bending moment M as $M = Fc/2$. Then, half of the strut, either OA or OB, can be considered as a cantilever beam subjected to a tip force F. The transverse deflection is given by

$$\delta = \frac{F\left(\frac{c}{2}\right)^3}{3E_s I} \tag{3}$$

where I, the moment of inertia of the strut cross-section, is given by $I = \frac{h^4}{12}$. The macroscopic shear stress τ^* is related to the shear force F as

$$\tau^* = \frac{F}{c^2} \tag{4}$$

The macroscopic shear strain γ^* can be calculated as

$$\gamma^* = \frac{2\delta}{(c/2)} = \frac{4\delta}{c} \tag{5}$$

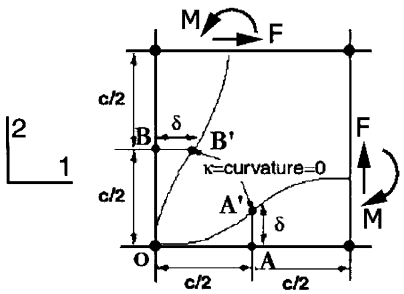

Fig. 4. Deformed shape of struts in an open-cell foam subjected to uniform macroscale shear stresses.

The shear modulus of the foam G_{12}^* is defined as the ratio of the macroscopic shear stress τ^* and macroshear strain γ^*. Then from Eqs. (4) and (5) we obtain

$$G_{12}^* = \frac{\tau^*}{\gamma^*} = \frac{1}{2} E_s \left(\frac{h}{c}\right)^4 \tag{6}$$

From the expressions for E_1^* and G_{12}^* a relationship between the shear modulus and the Young's modulus can be derived as

$$\frac{E_1^*}{G_{12}^*} = 2\left(\frac{c}{h}\right)^2 \tag{7}$$

Due to the symmetry of the structure it is obvious that $E_2 = E_3 = E_1$ and $G_{23} = G_{31} = G_{12}$. Further, all Poisson's ratios referred to the principal material directions, v_{12}, v_{23}, and v_{31}, are also approximately equal to zero.

The relative density ρ^*/ρ_s, where ρ_s is the solid density or the density of the strut material, is a measure of solidity of the cellular material. The density ρ^* of the foam can be obtained from the mass m and volume V of the material in a unit-cell. Basically, there are three struts, each of length c, within a unit-cell. Therefore, their volume will be equal to $3ch^2$. In order to be accurate, we can subtract the two overlapping volume h^3 each, at the intersection of the struts. Then the mass within a unit-cell will be equal to $\rho_s(3h^2c - 2h^3)$ and the volume of the unit-cell is c^3. Then a relation between the foam density ρ^* and the solid density ρ_s can be derived as:

$$\frac{\rho^*}{\rho_s} = \frac{\frac{\rho_s\left(3h^2c-2h^3\right)}{c^3}}{\rho_s} = 3\left(\frac{h}{c}\right)^2 - 2\left(\frac{h}{c}\right)^3 \tag{8}$$

If the aspect ratio of the strut $h/c \ll 1$, then the relative density can be approximated as

$$\frac{\rho^*}{\rho_s} \approx 3\left(\frac{h}{c}\right)^2 \tag{9}$$

2.2. Comparison of analytical models and finite element models

Although the aforementioned model for Young's modulus is simple and straightforward, the model for shear modulus needs to be compared with other approaches in order to make sure that the assumptions about the periodic boundary conditions are correct. In order to accomplish this purpose a portion of the foam was modeled using finite elements. Each strut was modeled as an Euler–Bernoulli beam with two nodes and three degrees of freedom, u_1, u_2 and θ, at each node. Each beam element has three integration points. Although we could have modeled one unit-cell with periodic boundary conditions, e.g., Marrey and Sankar (1995), a larger portion of the cellular medium was modeled, as the computational cost is not very high in the present case.

The model shown in Fig. 5 consists of 100×100 cells. The cell length c of the unit-cell is 200 μm and the strut is assumed to have a square cross-section with a side equal to 20 μm. A uniform displacement ($\delta = 0.01$ m) is applied at nodes on the top edge of the model. The total force in the 2-direction is computed from the FE results. The average tensile stress (macrostress σ_{22}) can be obtained by

$$\sigma_{22}^* = \frac{\sum F_2}{Lc} \tag{10}$$

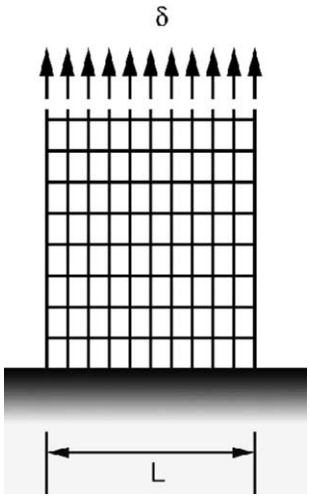

Fig. 5. Schematic of the FE model of the foam. A vertical displacement δ is applied at nodes on the top edge of the foam to simulate uniform tension.

where the $\sum$ sign denotes summation of all nodal forces acting on the boundary nodes where the displacements are prescribed and L is the width of the foam considered in the FE model (see Fig. 5). The Young's modulus E_2^* of foam can be determined by the stress–strain definition as

$$E_1^* = \frac{\sigma^*}{\varepsilon^*} = \frac{\sigma_{22}^*}{(\delta/L)} \tag{11}$$

For the case considered the FE model gave a value $E_1^* = 2.09$ GPa and the analytical model Eq. (2) yielded a value of 2.07 GPa. The difference of results is 1%.

To estimate the shear modulus by the FE method, a constant horizontal displacement u_s is applied to all the nodes on the topside of the foam as shown in Fig. 6. The shear stress τ^* can be obtained by the sum of reaction forces F divided by the area of the top surface:

$$\tau^* = \frac{\sum F_1}{Lc} \tag{12}$$

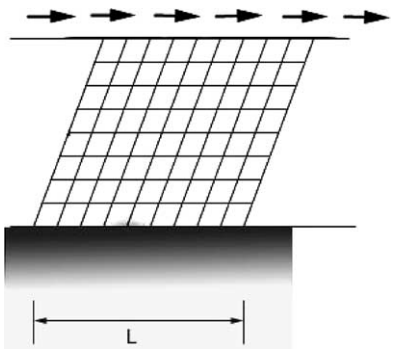

Fig. 6. Schematic of shear deformation in the open-cell foam.

where L is the length of the foam considered in the FE model and c is the unit-cell dimension. The shear strain γ^* can be calculated as

$$\gamma^* = \frac{u_s}{L} \tag{13}$$

Thus, shear modulus G_{12}^* of the foam can be estimated as the ratio of shear stress τ^* and shear strain γ^*, i.e. $G_{12}^* = \frac{\tau^*}{\gamma^*}$. Substituting for the shear stress and shear strain from Eqs. (12) and (13), respectively, we obtain

$$G^* = \frac{\sum F_1}{u_s c} \tag{14}$$

From the finite element analysis, the shear modulus of the foam was estimated as 10.25 MPa. The analytical model (Eq. (6)) yields a value of 10.35 MPa. The difference between the two results is about 1%. The FE model is slightly compliant because of lack of constraints on the vertical sides. Applying periodic boundary conditions (Marrey and Sankar, 1995) would have yielded values closer to the analytical solution.

3. Finite element based micromechanics for fracture toughness

In this section, we describe a finite element based micromechanics model for estimating the fracture toughness of the cellular solid. The crack is assumed to be parallel to one of the principal material axes, and Mode I, Mode II and mixed mode fracture conditions are considered. To determine the fracture toughness, a small region around the crack tip is modeled using beam elements, and a constant mode mixity K_I/K_{II} is considered. The boundary of the cellular solid is subjected to displacement boundary conditions u_1 and u_2 corresponding to an arbitrary value of K_I (or K_{II}). The rotational degree of freedom at each node of the beam element on the boundary of the solid is left as unknown and no couples are applied at these nodes. The calculation of boundary displacements for a given stress intensity factor is described in Section 3.1.

3.1. Boundary displacements near the crack tip

The displacement components in the vicinity of a crack tip in a homogenous orthotropic material are derived in Appendix A and they are as follows (Sih and Liebowitz, 1968):

The displacement filed near the crack tip for Mode I:

$$\begin{aligned} u_1 &= K_I\sqrt{\frac{2r}{\pi}}\mathrm{Re}\left\{\frac{1}{s_1-s_2}\left[s_1p_2(\cos\theta+s_2\sin\theta)^{1/2}-s_2p_1(\cos\theta+s_1\sin\theta)^{1/2}\right]\right\} \\ u_2 &= K_I\sqrt{\frac{2r}{\pi}}\mathrm{Re}\left\{\frac{1}{s_1-s_2}\left[s_1q_2(\cos\theta+s_2\sin\theta)^{1/2}-s_2q_1(\cos\theta+s_1\sin\theta)^{1/2}\right]\right\} \end{aligned} \tag{15}$$

The displacement filed near the crack tip for Mode II:

$$\begin{aligned} u_1 &= K_{II}\sqrt{\frac{2r}{\pi}}\mathrm{Re}\left\{\frac{1}{s_1-s_2}\left[p_2(\cos\theta+s_2\sin\theta)^{1/2}-p_1(\cos\theta+s_1\sin\theta)^{1/2}\right]\right\} \\ u_2 &= K_{II}\sqrt{\frac{2r}{\pi}}\mathrm{Re}\left\{\frac{1}{s_1-s_2}\left[q_2(\cos\theta+s_2\sin\theta)^{1/2}-q_1(\cos\theta+s_1\sin\theta)^{1/2}\right]\right\} \end{aligned} \tag{16}$$

In deriving the above expressions, the crack is assumed to be parallel to the 1-axis, and r–θ is the polar coordinate system situated at the crack tip. The complex parameters p, q, and s depend on the elastic constants of the homogeneous orthotropic material as described in Appendix A.

3.2. Finite element model

The commercial program ABAQUS™ is used to perform the finite element analysis. A portion of the foam surrounding the crack tip is modeled using beam finite elements as shown in Fig. 7. The displacement boundary conditions for the FE model are determined from the expression for boundary displacements described in the previous section. The crack in the FE model is created by removing the beam elements along the line of the crack behind the crack tip.

To reduce the modeling cost, a FORTRAN code was written to generate nodal and element properties with user specified unit-cell configuration. The code calculates boundary displacements at corresponding boundary nodal coordinates. After execution, it exports an ABAQUS input file so that the ABAQUS can read the input directly.

The maximum tensile stress in the struts is calculated from the finite element method. The FE analysis outputs axial force, bending moment and shear force at each node of the beam elements, and the maximum tensile stress was calculated using a separate program. Usually the maximum stress occurs at the crack tip strut. It should be noted that the stresses in the struts vary linearly with respect to the applied stress intensity factor K_I (or K_{II}). Since we know the strength of the strut material, the value of K_I (or K_{II}) that will cause rupture of the strut can be estimated. And then, it is taken as the fracture toughness of the cellular solid. It should be mentioned such scaling is possible because we assume linear elastic behavior of the strut material and hence that of the foam. If the strut material undergoes inelastic behavior, then an iterative method will have to be used to determine the stress intensity factor that will cause the failure of the crack-tip strut.

Before we describe an analytical model for estimating the fracture toughness, we will discuss the results from the FE simulation. At first, we will check the validity of applying continuum fracture mechanics. It was found that a model consisting of 100×100 cells (total 10,000 cells) gave a converged result for fracture toughness and the same model is used throughout the study.

3.3. Convergence analysis for mode I

The convergence analysis is performed to evaluate the variation of fracture toughness with various sizes of foam models, 12 mm × 12 mm (3600 cells), 20 mm × 20 mm (10,000 cells), 40 mm × 40 mm (40,000 cells)

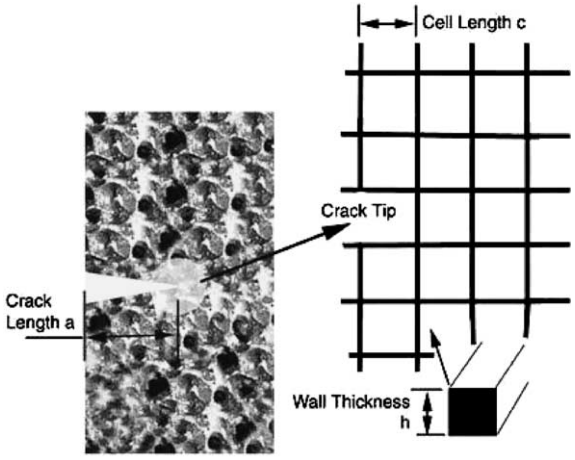

Fig. 7. Open-cell foam model with a crack.

and 80 mm × 80 mm (160,000 cells). In the convergence analysis the length of the unit-cell was taken as 200 μm and the cell wall thickness as 20 μm.

The values of fracture toughness computed from various size models are plotted in Fig. 8 as a function of number of cells in the model. As the model size increases, fracture toughness converges to a value approximately equal to 0.467 MPa$\sqrt{\text{m}}$ as shown in Fig. 8. The difference in results for models containing 10,000 and 160,000 cells is about 2.7%. Therefore, the 10,000-cell model is chosen for further analysis to maintain reasonable accuracy but with less CPU time. For the 10,000-cell model, a computer with 1.7 GHz Intel Pentium® 4 takes $13\frac{1}{2}$ min to complete the job, but the 160,000 cells takes more than 2 h.

The axial stresses in the beam element cross-sections ahead of the crack tip are shown in Fig. 9. Smaller size models produce slightly higher axial stresses in the crack tip element. Away from the crack tip,

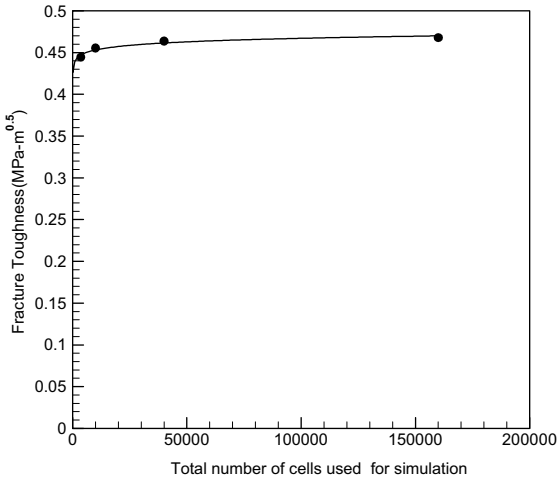

Fig. 8. Variation of fracture toughness with number of cells in the model.

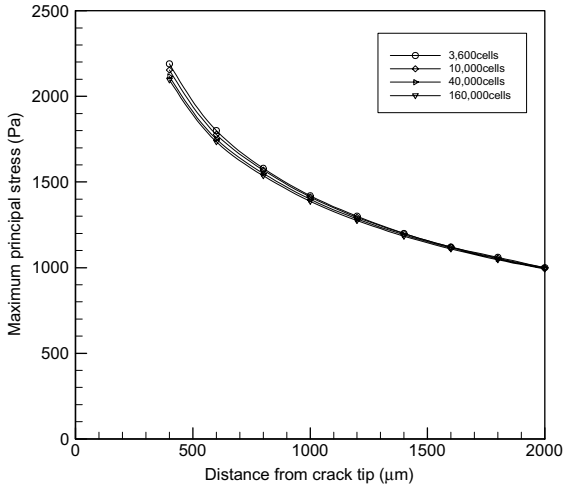

Fig. 9. Variation of axial stresses in the beam elements as a function of distance from the crack tip for various size models.

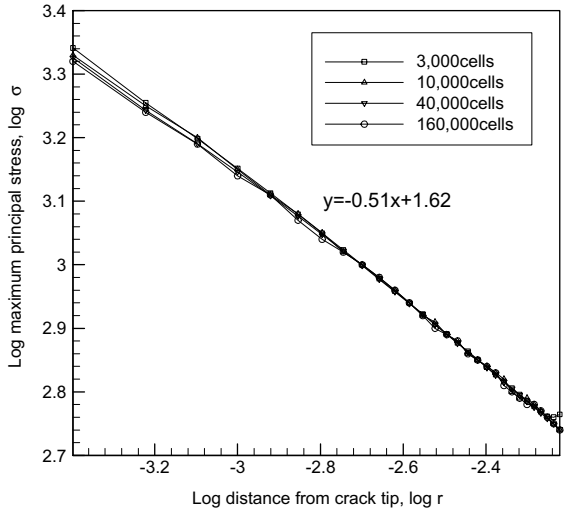

Fig. 10. Logarithmic plot of axial stresses ahead of the crack tip for various size models.

differences in axial stresses become insignificant for different size models. The log–log plot of stress variation ahead of the crack tip is shown in Fig. 10. One can note that in Fig. 10 the slope of the straight line is approximately equal to -0.5 indicating the existence of an inverse square root singularity at the crack tip. A least-square fit of the stress distribution results in

$$\sigma = \frac{41.69}{\sqrt{r}} \tag{17}$$

where r is the distance from the crack tip. Using the relation between micro and macrostresses in Eq. (1), Eq. (17) can be written as

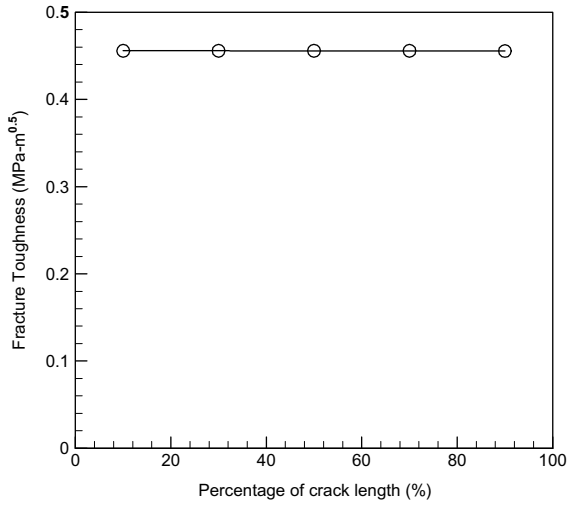

Fig. 11. Predicted fracture toughness for various crack lengths.

$$\sigma_{22}^{*} = \frac{1.05}{\sqrt{2\pi r}} \tag{18}$$

which indicates that the approximate stress intensity factor in macroscale is equal to 1.05, which is close the unit stress intensity factor used in imposing the boundary conditions.

If the fracture toughness estimated by using the present method is truly a material (macroscopic) property, then it should be independent of the crack length. Hence, the crack length was varied in the micromechanical method. The results are shown in Fig. 11. The predicted fracture toughness is plotted as a function of the crack length. Note that the size of the foam was kept constant and the crack length was varied. In Fig. 11, the crack length is shown as a percentage of the width of the foam. The result clearly shows that the fracture toughness is independent of the crack length. Furthermore the crack tip singularity was equal to $-1/2$ (see Eq. (18)), which is the theoretical value for homogeneous orthotropic materials. Thus one can conclude that although the foam is a cellular material consisting of discrete struts, on a macroscale the fracture behavior is similar to that of a homogeneous orthotropic continuum. Hence one can calculate or measure fracture toughness for such cellular materials.

3.4. Mode I fracture toughness of open cell foam

Since the relative density depends on the length of the strut c and the strut cross-sectional dimension h, the density was varied in two different ways. In the first case, c was varied and h was kept constant. In the second case, h was varied while c was constant.

The results of the FE simulation are axial force, bending moment and shear force in each element, which are used to calculate the maximum principal stress at the crack tip, and then the fracture toughness. A sample stress distribution due to Mode I loading is shown in Fig. 12.

The variation of Mode I fracture toughness with relative density is shown in Fig. 13. A least square power law fitting yielded

$$\begin{aligned} K_{\mathrm{Ic}} &= 1.961\left(\frac{\rho^{*}}{\rho_s}\right)^{1.045} \quad \text{constant cell length,} \quad c = 200\ \mu\mathrm{m} \\ K_{\mathrm{Ic}} &= 7.82\left(\frac{\rho^{*}}{\rho_s}\right)^{0.788} \quad \text{constant strut thickness,} \quad h = 20\ \mu\mathrm{m} \end{aligned} \tag{19}$$

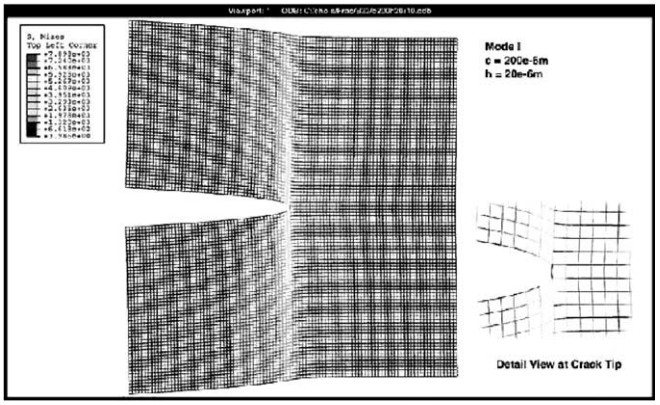

Fig. 12. Deformation of the foam subjected to Mode I loading (cell length $c = 200$ μm, strut thickness $h = 20$ μm).

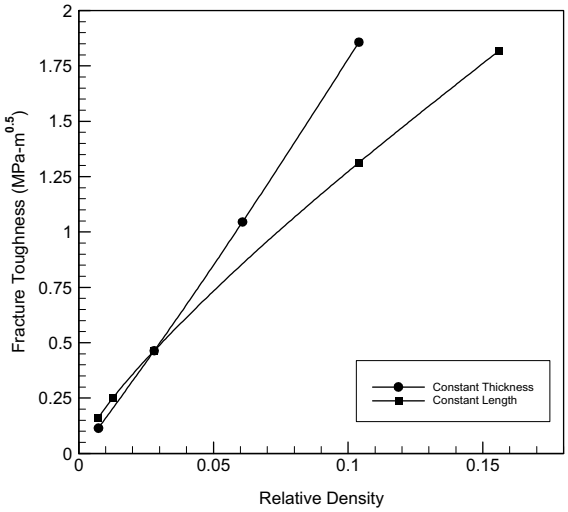

Fig. 13. Mode I fracture toughness as a function of relative density for two cases: constant unit-cell length and constant strut thickness.

For very low relative densities (0.01–0.04), the fracture toughness seems to be independent of the cell size or strut size. However, at higher densities, thicker struts yielded higher fracture toughness compared to the foams with thinner struts but of same density.

3.5. Mode II fracture toughness of open cell foam

The analysis of Mode II fracture toughness is very similar to that of Mode I fracture analysis presented in the preceding section. An example of deformation in Mode II is depicted in Fig. 14. Unlikely Mode I fracture, the boundary displacements are not symmetric about the crack plane as shown. The displacement field for Mode II case is given by Eq. (16). The variation of Mode II fracture toughness with relative density for both constant strut thickness and constant cell size are shown in Fig. 15. The results of Mode II fracture

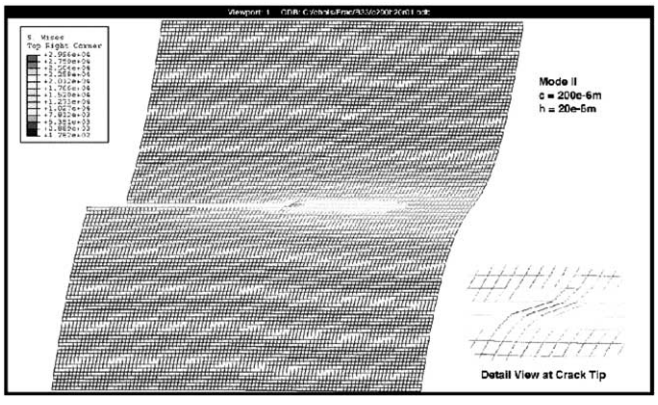

Fig. 14. Deformation of the foam subjected to Mode II loading (cell length $c = 200$ μm, strut thickness $h = 20$ μm).

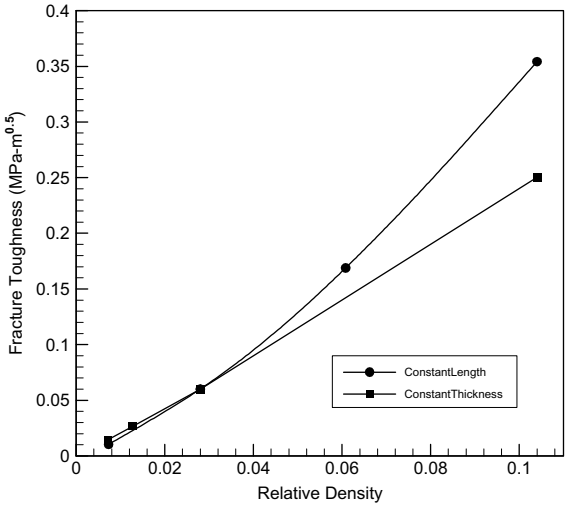

Fig. 15. Mode II fracture toughness as a function of relative density for two cases: constant unit-cell length (200 μm) and constant strut thickness (20 μm).

toughness shown in Fig. 15 were fitted to a power law using least square error procedure. The results are as follows:

$$\begin{aligned} K_{\mathrm{IIc}} &= 6.95\left(\frac{\rho^*}{\rho_s}\right)^{1.32} \quad \text{constant cell length, } c = 200\ \mu\text{m} \\ K_{\mathrm{IIc}} &= 2.76\left(\frac{\rho^*}{\rho_s}\right)^{1.07} \quad \text{constant strut thickness, } h = 20\ \mu\text{m} \end{aligned} \tag{20}$$

As before the Mode II fracture toughness seems to be independent of the cell size and strut thickness at low densities, but vary significantly with the dimensions at higher densities. A semi-empirical relation for Mode II fracture toughness is presented in Section 4.2.

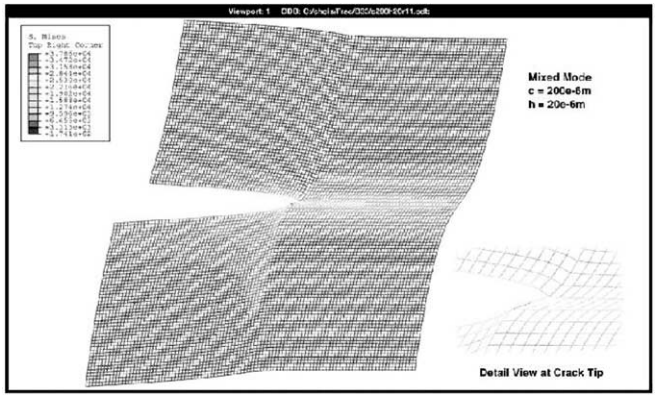

Fig. 16. Deformation of the foam subjected to mixed mode loading conditions ($c = 200$ μm, $h = 20$ μm).

3.6. Mixed mode fracture toughness

The procedures for mixed mode analysis is similar to that of Mode I and Mode II. A fixed K_I/K_{II} ratio is assumed and the boundary displacements were obtained as superposition of displacement given in Eqs. (15) and (16). An example of deformation in mixed mode is depicted in Fig. 16. The value of K_I (or K_{II}) that will cause rupture of the crack tip strut was calculated.

The results are shown in Fig. 17 for constant strut thickness and in Fig. 18 for constant cell size. It is found that the results can be expressed as

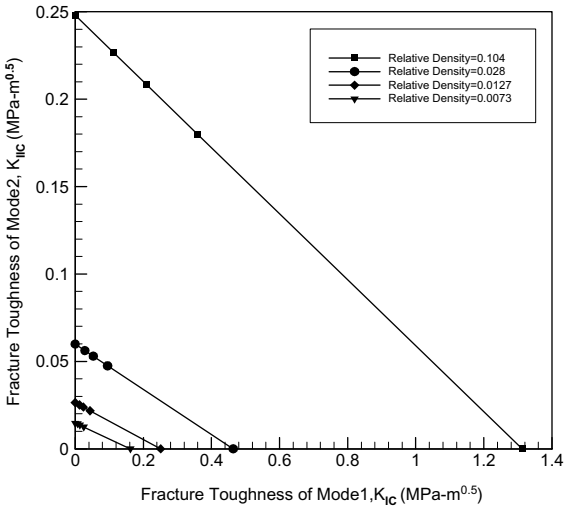

Fig. 17. Mixed-mode fracture toughness for various relative densities (constant strut thickness $h = 20$ μm).

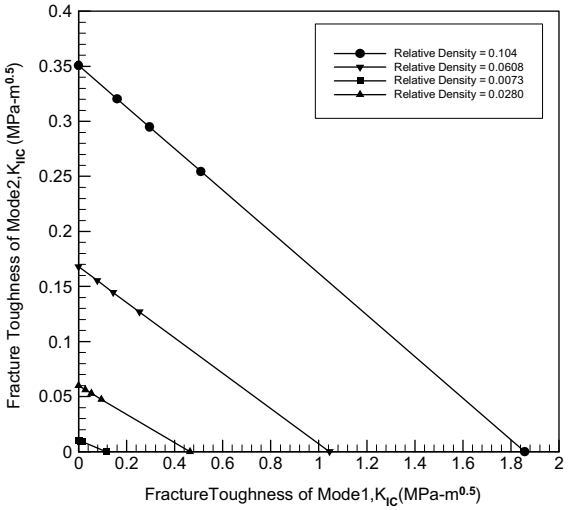

Fig. 18. Mixed-mode fracture toughness for various relative densities (constant cell length $c = 200$ μm).

$$\left(\frac{K_{\mathrm{I}}}{K_{\mathrm{Ic}}}\right)+\left(\frac{K_{\mathrm{II}}}{K_{\mathrm{IIc}}}\right)=1 \tag{21}$$

This result does not reveal any surprise as we are using stress based failure criterion for the struts and the usual linear superposition holds good.

4. Semi-empirical models for fracture toughness

4.1. Analytical model for mode I fracture toughness

In order to derive an analytical model for fracture toughness, the stress intensity factor of the homogeneous model should be related to the actual stresses in the crack tip ligament of the foam. This can be obtained by assuming that the internal forces and bending moment in the crack tip strut are caused by a portion of the crack tip stress field ahead of the crack tip in the homogeneous model as illustrated in Fig. 19.

Let us define a non-dimensional factor α that describes the effective length l as follows:

$$l=\alpha c \tag{22}$$

Previous researchers (e.g. Gibson and Ashby, 1988) have arbitrarily assumed that the effective length l is equal to the cell spacing c, i.e., $\alpha=1$. Because of the existence of the singularity, such assumption may not be valid. Furthermore, it could be a function of the foam density also. In this study we use the micromechanics results (Eq. (19)) to estimate the effective length more accurately. The ideal stress distribution σ_{22} ahead of crack tip is described as follows:

$$\sigma_{22}=\frac{K_{\mathrm{I}}}{\sqrt{2\pi r}} \tag{23}$$

where r is the distance from the crack tip. The axial force F in the crack tip ligament can be obtained by integrating σ_{22} over the effective length

$$F=c\int_0^l \sigma_{22}\,\mathrm{d}r=K_{\mathrm{I}}c\sqrt{\frac{2l}{\pi}} \tag{24}$$

Similarly the bending moment M in the crack tip strut is given by

$$M=c\int_0^l r\sigma_{22}\,\mathrm{d}r \tag{25}$$

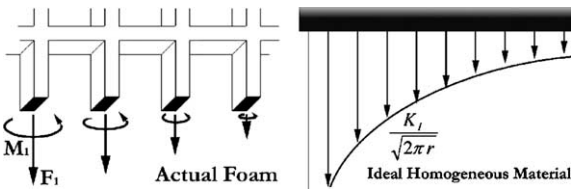

Fig. 19. Crack-tip forces and moments in the actual foam and corresponding crack tip stresses in the idealized homogeneous continuum.

Substituting for σ_{22} from Eq. (22), we obtain the expression for crack tip bending moment as

$$M = K_I \sqrt{\frac{2}{\pi}} \frac{l^{3/2}}{3} c \tag{26}$$

Assuming fracture occurs when the maximum bending stress equals the tensile strength of the ligament material, a relationship between the tensile strength and fracture toughness can be derived as

$$\sigma_u = \frac{M(h/2)}{(h^4/12)} + \frac{F}{h^2} = \frac{6M}{h^3} + \frac{F}{h^2} = \frac{K_{Ic} c}{h^2} \sqrt{\frac{2l}{\pi}} \left(1 + 2\frac{l}{h}\right) \tag{27}$$

In deriving Eq. (27) expressions for M and F in terms of K_{Ic} given in (24) and (26) have been used. By substituting for l in terms of α from Eq. (22), a relation between fracture toughness and tensile strength of the strut material can be derived as

$$K_{Ic} = \sigma_u \sqrt{c} \sqrt{\frac{\pi}{2}} \frac{h^2}{c^2} \frac{1}{\sqrt{\alpha}\left(1 + 2\alpha \frac{c}{h}\right)} \tag{28}$$

The results for K_{Ic} presented in Fig. 13 were used in conjunction with Eq. (28) to calculate the value of α for various cases. The results for α as a function relative density are plotted in Fig. 20. It may be noted that α increases with relative density and the variation can be accurately represented by a power law. Interestingly both constant wall thickness (constant h) case and the constant cell size case (constant c) we have studied so far fit accurately into a single power law. The effective length is about 9% of the cell spacing for low-density foam and about 23% for the high-density foam.

Thus one can consider the results presented in Eq. (19) as empirical formulas for fracture toughness, whereas Eq. (28) is semi-empirical in the sense that it is based on mechanistic approach.

4.2. Analytical model for mode II fracture toughness

The effective crack tip distance for Mode II can be derived following steps similar to that in the preceding section for Mode I.

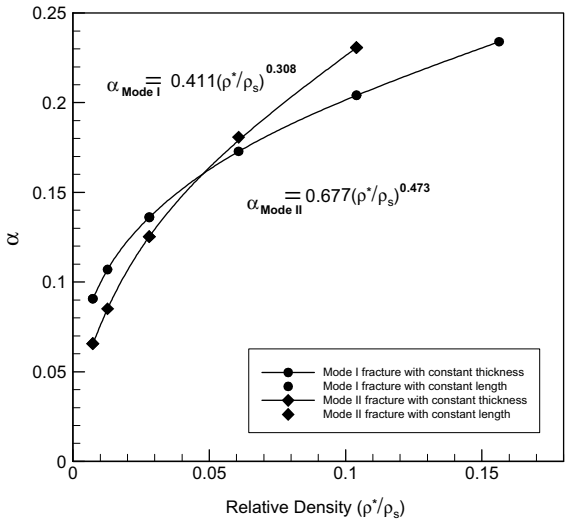

Fig. 20. Variation of α with relative density for Mode I and Mode II fracture. Both constant cell length case and constant strut thickness case follow the same equation.

The shear stress (τ_{12}) distribution ahead of the crack tip is given by:

$$\tau_{12} = \frac{K_{II}}{\sqrt{2\pi r}} \tag{29}$$

The total shear force F over the effective distance l can be derived as

$$F = c\int_0^l \tau_{12}\,\mathrm{d}r = K_{II}c\sqrt{\frac{2l}{\pi}} \tag{30}$$

The maximum bending moment in the crack tip element is the product of force F and the moment arm given by $c/2$:

$$M = K_{II}\sqrt{\frac{2l}{\pi}}\frac{c^2}{2} \tag{31}$$

The maximum bending stress is derived as

$$\sigma = \frac{6M}{h^3} = 3K_{II}\sqrt{\frac{2l}{\pi}}\frac{c^2}{h^3} \tag{32}$$

An expression for fracture toughness K_{II} in terms of strut tensile strength, strut dimensions and the effective distance can be derived as

$$K_{II} = \frac{\sigma_u h^3}{3c^2}\sqrt{\frac{\pi}{2l}} \tag{33}$$

Using $l = \alpha c$ in the above equation we obtain

$$K_{II} = \frac{\sigma_u h^3}{3c^2}\sqrt{\frac{\pi}{2\alpha c}} = \frac{\sigma_u h^3}{3c^{3/2}}\sqrt{\frac{\pi}{2\alpha}} \tag{34}$$

From Eq. (34) an expression for α can be derived as

$$\alpha = \left(\frac{\sigma_u h^3}{3K_{II}c^{3/2}}\sqrt{\frac{\pi}{2}}\right)^2 = \frac{\pi\sigma_u^2 h^6}{18K_{II}^2 c^5} \tag{35}$$

The constant α can be evaluated using the FE results of fracture toughness. The value of α as a function of relative density is plotted in Fig. 20. Again, it can be noted that a power law description is adequate for Mode II also. Further the value of α depends only on the relative density and not on individual cell or strut dimensions. It is about 7% of the strut spacing c for low-density foams and about 22% for high-density foams.

5. Mode I fracture toughness of inclined cracks

So far our attention has been focused on cracks parallel to the principal material direction. The next step will be to study cracks inclined at an angle to the principal material direction. The procedures for predicting the fracture toughness of angled cracks are very similar to those described in the preceding sections. The only change is in the material elastic constants, which have to be transformed from the material principal directions to the global x–y coordinate system where x-axis is aligned parallel to the crack.

The deformation in the vicinity of the crack tip under Mode I fracture for various crack angles are shown in Fig. 21. One can note the symmetric opening of the crack surfaces behind the crack tip. The variation of Mode I fracture toughness with crack orientation is shown in Fig. 22 for various relative densities. In all these cases the cell spacing was kept at 200 μm and the density was varied by changing the

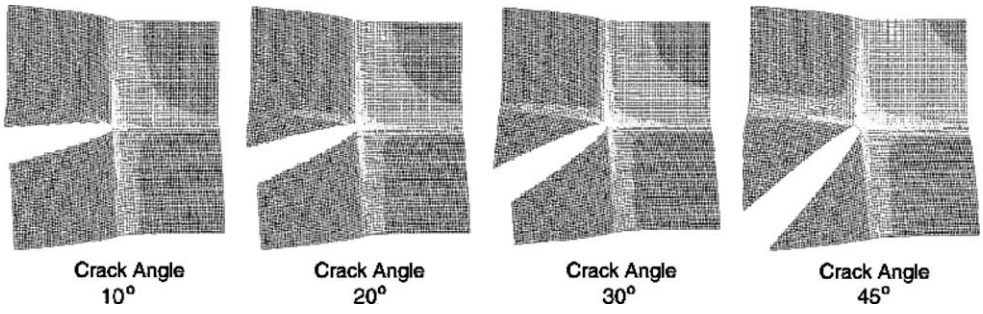

Fig. 21. Deformation of foam containing various angled cracks under Mode I loading.

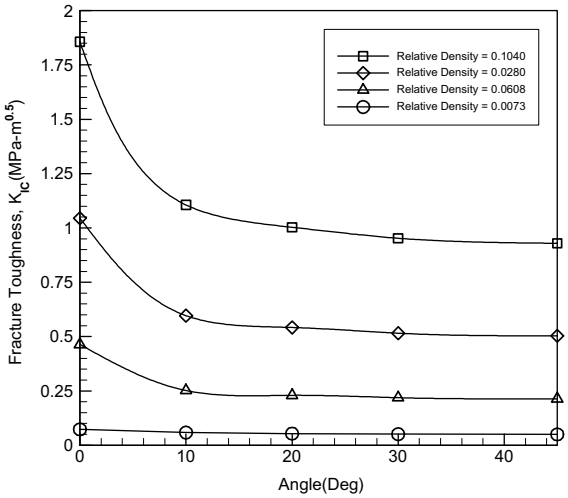

Fig. 22. Mode I fracture toughness for various cracks inclined to the principal material direction.

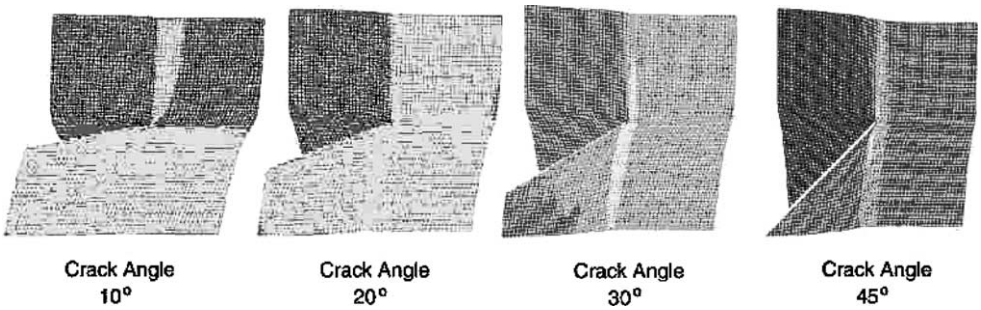

Fig. 23. Deformation of foam containing various angled cracks under Mode II loading.

strut cross-sectional dimension from 10 to 40 μm in steps of 10 μm. It may be noted that the K_{Ic} is maximum when the crack is oriented parallel to the principal material direction and it reduces by about 50% as the crack rotates by 45° to the principal direction.

The deformation under Mode II loading for various crack orientation is depicted in Fig. 23. The variation of Mode II fracture toughness with crack orientation is shown in Fig. 24 for various relative densities.

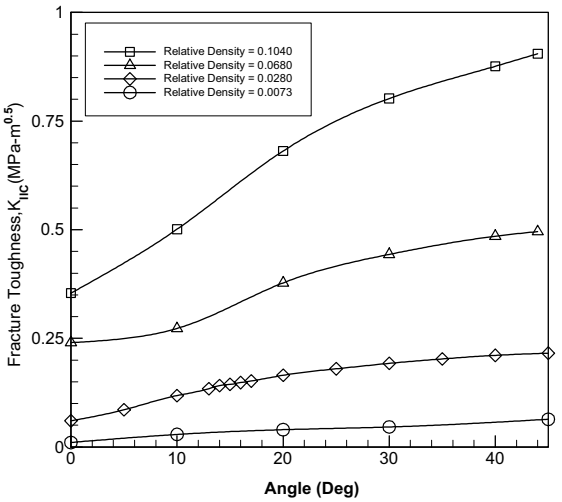

Fig. 24. Mode II fracture toughness for various cracks inclined to the principal material direction.

Again it is interesting to see that the crack surfaces do not open but slide indicating pure Mode II conditions. Mode II fracture toughness increases with crack angle and it reaches a maximum for cracks oriented at 45° to the principal material direction. Because of symmetry, the fracture toughness relations for both Mode I and Mode II in Figs. 22 and 24 are expected to be symmetric about $\theta = 45°$.

6. Summary and conclusions

A finite element based micromechanics method has been developed to determine the fracture toughness of cellular materials. A portion of the cellular medium surrounding the crack tip is modeled using beam finite elements. Displacement boundary conditions are applied such that they correspond to a given value of stress intensity factor in a homogeneous solid that has the same elastic constants as the cellular medium. The stresses developed in the beam elements (struts) are used to determine if the strut will break or not. From the results the fracture toughness of the cellular medium is estimated. It is shown that the value obtained is independent of the crack length indicating that the calculated value of the fracture toughness is truly a material property of the foam. The fracture toughness is a function of relative density only for low-density foams, however at higher densities it depends on the cell size and the strut cross-sectional dimensions. The concept of an effective length is introduced and empirical formulas for Mode I and Mode II fracture toughness have been derived. The locus of mixed mode fracture toughness follows a straight line between Mode I and Mode II fracture toughness values. Cracks at an angle to the principal material directions were studied. The mode I fracture toughness is maximum when the crack is parallel to the material principal direction and it is minimum when it is at 45°. The converse is true for Mode II fracture toughness. Future work will be concerned with developing analytical formulas for angled cracks and foams of different microstructures including functionally graded foams.

Acknowledgment

Thanks are due to Dr. Ajit Roy of Wright-Patterson Air Force Base for his guidance and technical discussions during the course of this project. Support from the NASA URETI Grant NCC3-994 managed by Glenn Research Center is also acknowledged.

Appendix A. Crack tip displacement fields for orthotropic materials

The open-cell foam is considered as an orthotropic material. The principal material directions are parallel to the 1 and 2 axes. The stress–stain relations in the 1–2 plane for the case of plane stress can be expressed as

$$\begin{Bmatrix} \varepsilon_1 \\ \varepsilon_2 \\ \gamma_{12} \end{Bmatrix} = [S]\{\sigma\} = \begin{bmatrix} \frac{1}{E^*} & -\frac{v}{E^*} & 0 \\ -\frac{v}{E^*} & \frac{1}{E^*} & 0 \\ 0 & 0 & \frac{1}{G^*} \end{bmatrix} \begin{Bmatrix} \sigma_1 \\ \sigma_2 \\ \tau_{12} \end{Bmatrix} \tag{A.1}$$

The stress–stain relation can be transformed from the 1–2 coordinate system to the x–y coordinate system by using transformation matrix $[T]$:

$$\begin{Bmatrix} \sigma_1 \\ \sigma_2 \\ \sigma_3 \end{Bmatrix} = [T] \begin{Bmatrix} \sigma_x \\ \sigma_y \\ \sigma_z \end{Bmatrix} \tag{A.2}$$

where the transformation matrix is defined as

$$[T] = \begin{bmatrix} \cos^2\theta & \sin^2\theta & 2\sin\theta\cos\theta \\ \sin^2\theta & \cos^2\theta & -2\sin\theta\cos\theta \\ -\sin\theta\cos\theta & \sin\theta\cos\theta & \cos^2\theta - \sin^2\theta \end{bmatrix} \tag{A.3}$$

and θ is the angle made by the 1-axis with the x-axis.

By applying the transformation matrix, the compliance matrix $[\overline{S}]$ in the x–y plane can be written as

$$\left[\overline{S}\right] = \begin{bmatrix} \overline{S}_{11} & \overline{S}_{12} & \overline{S}_{16} \\ \overline{S}_{12} & \overline{S}_{22} & \overline{S}_{26} \\ \overline{S}_{16} & \overline{S}_{26} & \overline{S}_{66} \end{bmatrix} = [T]^{\mathrm{T}}[S][T] \tag{A.4}$$

Explicit expressions for the components of $[\overline{S}]$ matrix are as follows:

$$\begin{aligned} \overline{S}_{11} &= S_{11}\cos^4\theta + (2S_{12} + S_{66})\sin^2\theta\cos^2\theta + S_{22}\sin^4\theta \\ \overline{S}_{12} &= S_{12}(\sin^4\theta + \cos^4\theta) + (S_{11} + S_{22} - S_{66})\sin^2\theta\cos^2\theta \\ \overline{S}_{22} &= S_{11}\sin^4\theta + (2S_{12} + S_{66})\sin^2\theta\cos^2\theta + S_{22}\cos^4\theta \\ \overline{S}_{16} &= (2S_{11} - 2S_{12} - S_{66})\sin\theta\cos^3\theta - (2S_{22} - 2S_{12} - S_{66})\sin^3\theta\cos\theta \\ \overline{S}_{16} &= (2S_{11} - 2S_{12} - S_{66})\sin^3\theta\cos\theta - (2S_{22} - 2S_{12} - S_{66})\sin\theta\cos^3\theta \\ \overline{S}_{11} &= 2(2S_{11} + 2S_{22} - 4S_{12} - S_{66})\sin^2\theta\cos^2\theta + S_{66}(\sin^4\theta + \cos^4\theta) \end{aligned} \tag{A.5}$$

The characteristic equation of the orthotropic material is given by Sih and Liebowitz (1968)

$$\overline{S}_{11}\mu^4 - 2\overline{S}_{16}\mu^3 + \left(2\overline{S}_{12} + \overline{S}_{66}\right)\mu^2 - 2\overline{S}_{26}\mu + \overline{S}_{22} = 0 \tag{A.6}$$

where the complex roots of the characteristic equation are given by μ_j $(j = 1, 2, 3, 4)$.

From the four roots, the two unequal roots with positive conjugate values are denoted by s_1 and s_2:

$$s_1 = \mu_1 = \alpha_1 + \mathrm{i}\beta_1, \quad s_2 = \mu_2 = \alpha_2 + \mathrm{i}\beta_2 \tag{A.7}$$

The constants p_j and q_j $(j = 1,2)$ are related to s_1 and s_2 as follows:

$$p_1 = a_{11}s_1^2 + a_{12} - a_{16}s_1, \quad p_2 = a_{11}s_2^2 + a_{12} - a_{16}s_2$$
$$q_1 = \frac{a_{12}s_1^2 + a_{22} - a_{26}s_1}{s_1}, \quad q_2 = \frac{a_{12}s_2^2 + a_{22} - a_{26}s_2}{s_2} \tag{A.8}$$

The displacement field in the vicinity of the crack tip is a function of the orthotropic material parameters p_1, p_2, q_1, q_2, s_1 and s_2 shown in Eqs. (15) and (16).

References

Gibson, L.J., Ashby, M.F., 1988. Cellular Solids: Structure and Properties, second ed. Cambridge University Press, Cambridge, United Kingdom.

Li, K., Gao, X.-L., Roy, A.K., 2003. Micromechanical analysis of three-dimensional open-cell foams using the matrix method for space frame structures. In: Proceedings of the Fourteenth International Conference on Composite Materials, Paper Number 1404, Society of Manufacturing Engineers, Dearborn, Michigan.

Sihn, S., Roy, A.K., 2003. Parametric study on effective Young's modulus and Poisson's ratio of open-cell carbon foam. In: Proceedings of the Fourteenth International Conference on Composite Materials, Paper Number 1279, Society of Manufacturing Engineers, Dearborn, Michigan.

Choi, S., Sankar, B.V., July 2003. A micromechanics method to predict the fracture toughness of carbon foam. In: Proceedings of the Fourteenth International Conference on Composite Materials, Paper Number 1355, Society of Manufacturing Engineers, Dearborn, Michigan.

Marrey, R.V., Sankar, B.V., October 1995. Micromechanical Models for Textile Structural Composites, NASA Contractor Report 198229.

Sih, G.C., Liebowitz, H., 1968. Mathematical theories of brittle fracture. In: Liebowitz, H. (Ed.), Fracture—An Advanced Treatise, vol. 2. Academic Press, New York, pp. 67–190.